

# Effect of Aircraft Banking on ARAIM Performance

R. Eric Phelts, Juan Blanch, Kazuma Gunning, Todd Walter, Per Enge  
*Stanford University*

## ABSTRACT

Significant differences in the quality of measurements made by a ground receiver compared to an avionics receiver may arise due to the dynamics of the aircraft. Banking for turns, in particular, can cause the GNSS measurements to be adversely affected in a number of ways. This may include adverse effects on multipath, satellite outages, and cycle slips.

This paper uses flight data to examine the effects that aircraft banking has on expected multipath error, the likelihood of satellite outages, and the likelihood of cycle slips. It then uses these insights to estimate effects on ARAIM availability due to outages that may occur during banking conditions. It is believed these assessments can allow for an improved understanding of GNSS measurement sensitivity to banking and also of potential effects on ARAIM availability during these maneuvers.

## BACKGROUND

Advanced Receiver Autonomous Integrity Monitoring (ARAIM) is being developed to extend RAIM to multiple constellations and dual frequency, with the goal of providing first an increased coverage of horizontal guidance, and later, worldwide coverage of vertical guidance for aircraft. Availability simulations have shown that ARAIM based on L1-L5 GPS-E1-E5a Galileo would provide global coverage of LPV-200 [1]. These simulations rely on a set of assumptions on the new GNSS signals and the behavior of the airborne receiver.

A preliminary assessment of these assumptions was begun in [2] and [3] with a limited amount of data. This work extends this analysis to a much larger data set and in the presence of larger dual frequency constellations (e.g., Galileo). In particular, this work examines ARAIM performance sensitivity to the

underlying assumptions of “straight and level” flight conditions, or that aircraft dynamics have negligible effects on performance.

## METHODOLOGY

Flight data collected over a period of approximately two years was used to evaluate underlying ARAIM assumptions on multipath error bounding, cycle slips, and momentary outages due to aircraft banking using multiple GNSS constellations and multiple frequencies. A multi-constellation, multi-frequency receiver (Trimble BX935-INS) tracked all the current GNSS constellations, satellites, and civil signals; in particular GPS, (L1 C/A, L1C, L2 (semi-codeless), L2C, and L5) and Galileo (E1 and E5a-E5b). This receiver is installed in a Global 5000 jet owned and operated by the William J. Hughes FAA Technical Center and continuously records and stores GNSS measurements. To date, this data collection effort includes many hours of data recorded over approximately 50 flights from September 2016 to October 2017.

### *Banking Angle Estimation*

To analyze the effects of aircraft banking, the banking angle is required to determine the “apparent” or body frame-based elevation angle of each satellite relative to the aircraft. Assuming the aircraft velocity is always aligned with the body axis of the aircraft and that the turns are coordinated (i.e., no “side slip”), carrier-phase GNSS measurements can be used approximate this reasonably well. (Note that an IMU would provide more precise measure of the aircraft attitude, however this provides a satisfactory estimate for the trends analyzed herein.)

To this end, the body frame basis must first be defined and the centripetal acceleration of the aircraft computed from carrier phase measurements.

The body frame is approximated by the basis vectors  $(u, v, w)$ , where

$$u = \frac{\text{velocity}}{|\text{velocity}|} \quad (1)$$

$$w = \frac{\text{accel}_{\text{accross}}}{|\text{accel}_{\text{accross}}|} \quad (2)$$

$$v = w \times u \quad (3)$$

The apparent acceleration of the aircraft is then

$$\text{accel}_{\text{app}} = \frac{d(\text{velocity})}{dt} - \text{gravity} \quad (4)$$

And the centripetal acceleration ( $\text{accel}_{\text{accross}}$ ) is simply the apparent acceleration in the direction of the turn.

$$\text{accel}_{\text{accross}} = \text{accel}_{\text{app}} - (u \cdot \text{accel}_{\text{app}}) * u \quad (5)$$

Then the banking angle is determined as

$$\text{banking angle} = \sin^{-1}(w \cdot u_N) \quad (6)$$

In the above equation,  $w$  is the vector defining the plane of the body frame of the aircraft and  $u_N$  is the vector defining the vertical. (See Figure 1.)

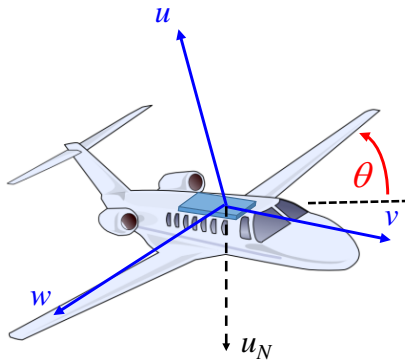


**Figure 1.** Illustration of body frame basis vectors and banking angle,  $\theta$ .

Figures 2 and 3 below show examples of the carrier phase-based speed and acceleration for two consecutive flights.

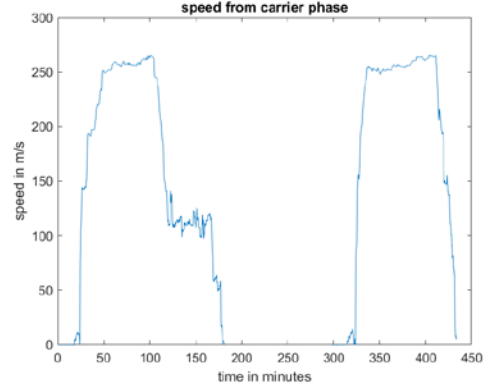


**Figure 2.** Carrier phase based speed from two flights.

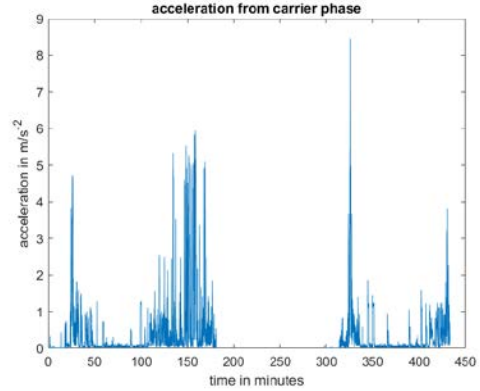


**Figure 3.** Carrier phase based acceleration from two flights.

An example of the computed banking angle during one portion of a flight is shown in Figure 4. The (assumed) maximum allowable banking angle of  $30^\circ$  is indicated for reference.

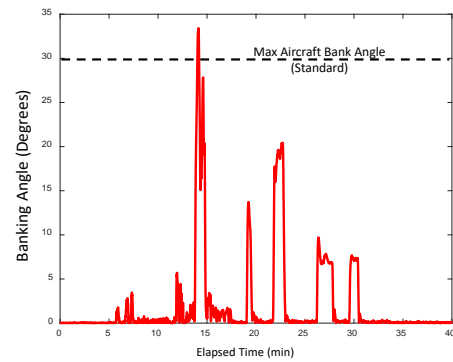


**Figure 4.** Example detail of computed banking angle estimate.  $30^\circ$  (max) angle indicated.

The line of sight (LOS) vectors for each satellite can then be projected into the frame of the aircraft and the body frame elevation determined according to Equations 7 and 8.

$$LOS_{aircraft} = \begin{bmatrix} u^T \\ v^T \\ w^T \end{bmatrix} LOS_{ENU} \quad (7)$$

$$elev_{aircraft} = \sin^{-1}(LOS_{aircraft,3}) \quad (8)$$

Figure 5 shows an example of the standard GNSS East-North-Up (ENU) elevation angle compared to the body-frame elevation angle for PRN 27. When the aircraft banks away from a satellite, its body frame elevation angle “appears” to decrease its elevation and goes below the ENU angle. When it banks toward a satellite, it appears to increase its elevation angle. Note that assuming a 30° maximum bank angle, a 5° ENU mask angle corresponds to a minimum body frame elevation angle of -25 degrees.

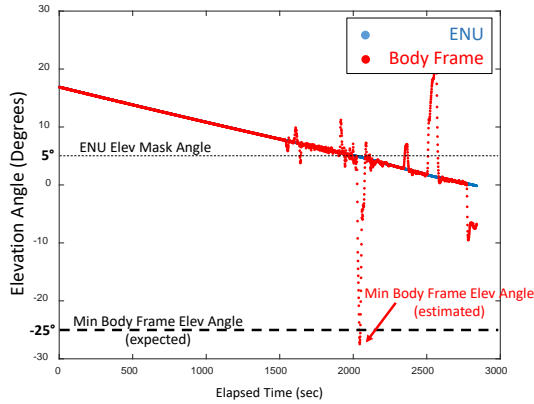


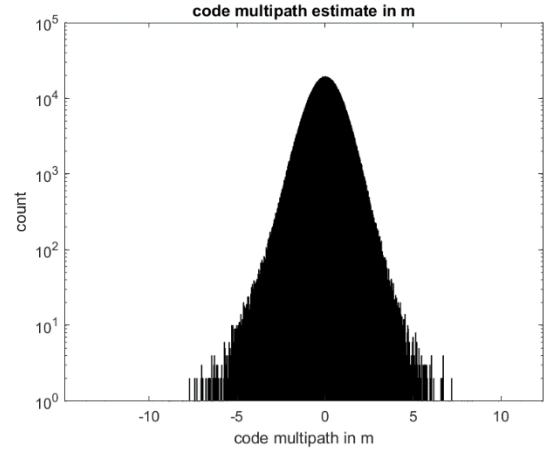
**Figure 5.** Body Fame vs ENU elevation for a satellite

## ANALYSIS AND RESULTS

### *Effect on Multipath Magnitude*

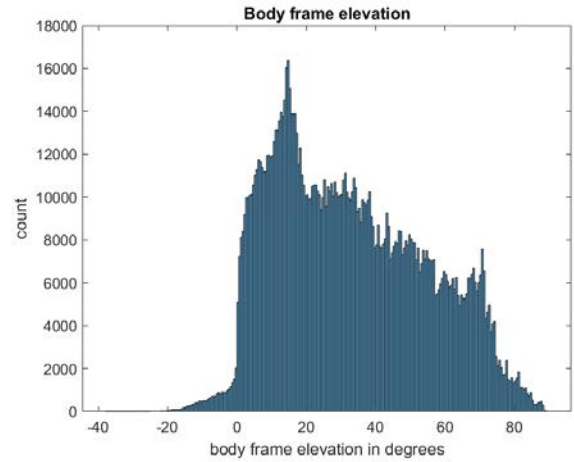
The body frame elevation of the satellites can be used to analyze its correlation with the magnitude of the code multipath. Code multipath is estimated using carrier leveling as described in [3]. Arcs free of cycle clips of at least 100 seconds in length were used to generate Figure 6, which plots a histogram of the raw, unsmoothed code multipath on GPS L1-L5 processed

from 36 flights. The minimum error was -13.5 m and the maximum was 11.1 m.



**Figure 6.** Histogram for code multipath estimated (GPS L1-L5)

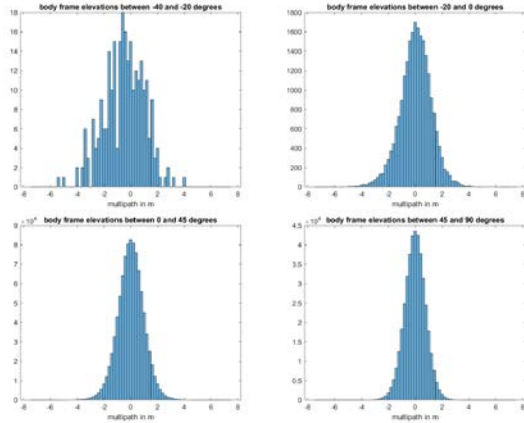
Figure 7 plots a histogram of all the raw measurements—1387913 samples (at 1 Hz)—as a function of body frame elevation angle. As expected, since banking is relatively rare, the overwhelming majority of the measurements occurs at apparent elevation angles above zero. Accordingly, the fewest measurements are available for the smallest body frame elevation angles.



**Figure 7.** Body frame elevation distribution

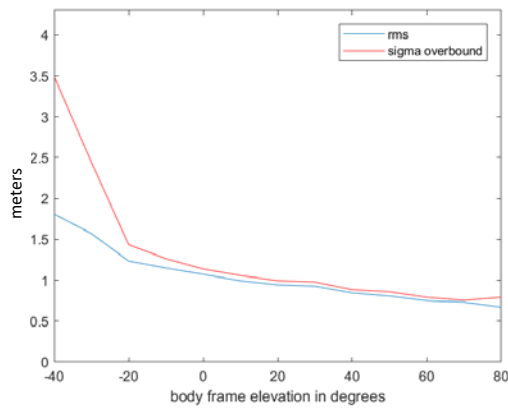
To measure the effect of banking angle on the multipath error, only satellites with an ENU elevation above a 5° mask are considered. Satellites below 5 degrees have a lower SNR, and are not expected to be to be tracked [3].

Figure 8 shows histograms for multipath data grouped into 4 bins: -40 to -20, -20 to 0, 0 to 45, and 45 to 90 degrees. The distributions at lower elevations are noticeably wider than at higher elevations, which indicates a body frame elevation dependency.



**Figure 8.** Multipath histograms grouped by body frame elevation (GPS L1-L5)

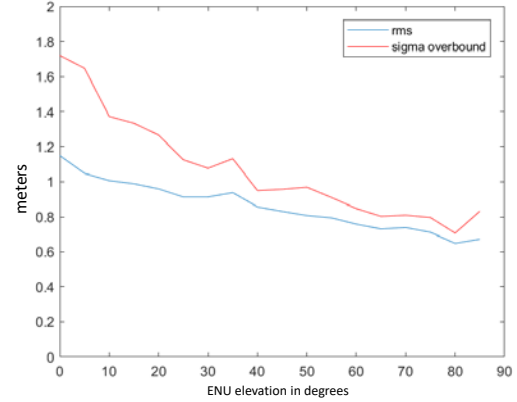
Figure 9 plots the multipath error and the corresponding overbound as a function of body frame elevation angles. The overbound was computed up to the 99<sup>th</sup> percentile. (This was limited due to insufficient data in the lower bins.) There is a ratio of more than 3-to-1 between the overbound below 0 degrees and below as compared to the highest body frame elevations. However, some of this is due to the ENU elevation dependence.



**Figure 9.** Multipath magnitude as a function of body frame elevation (GPS L1-L5)

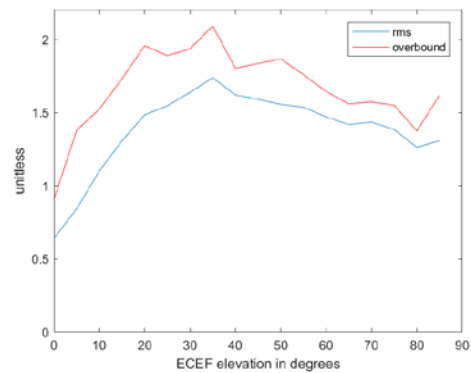
Figure 10 plots the multipath error and the corresponding overbound as a function of ENU elevation angle. For these results, only data

corresponding to level flight was used, and the overbound was computed up to the 99.95<sup>th</sup> percentile. There is a ratio of more than 2 to 1 between the multipath overbound at 0 degrees elevation and at 90. However, the elevation dependent error model is supposed to account for this dependence.



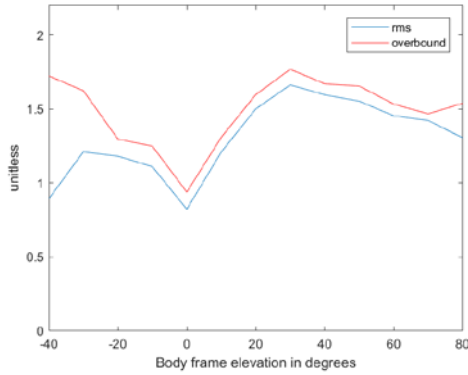
**Figure 10.** Multipath magnitude as a function of ENU elevation (GPS L1-L5)

To assess how much the ARAIM user (ENU elevation-based) multipath error model accounts for the elevation dependence, it was used to normalize the previous results. (This model is defined in [2] and [4].) Figure 11 plots the model-normalized multipath error for the ENU elevation angle for GPS L1-L5. We note that the model assumes 100 s carrier smoothing, so it is expected that this model will underestimate the code multipath, (since we are evaluating unsmoothed code). What is important here is that the model appears to remove the elevation dependence. Notably, below 20 degrees, the error model appears to be more conservative relative to how it performs at higher elevation angles.



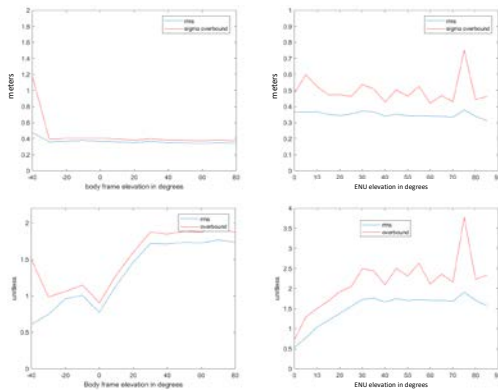
**Figure 11.** Normalized multipath as a function of ENU elevation (GPS L1-L5)

Figure 12 plots the model-normalized multipath error as a function of body frame elevation angle for GPS L1-L5. Here we see that the model performs similarly at both lowest and highest elevations. Below 0 degrees, the increase in multipath is somewhat accounted by the error model elevation dependence because satellites with negative body frame elevation typically have low elevations. This suggests the dynamics of the aircraft have relatively little effect on the multipath relative to what the ENU elevation-based multipath model expects.



**Figure 12.** Normalized multipath as a function of body frame elevation (GPS L1-L5)

To investigate further, the four plots of Figure 13 were generated like the ones in Figures 16 to 19 for GPS L1 only. There is some elevation dependence for the body frame elevation, but none is apparent in ENU elevation. As a consequence, the normalized multipath shows tighter distributions at lower elevations. These plots strongly suggest that the multipath error model somewhat overestimates the elevation dependence at low (ENU) elevation angles.



**Figure 13.** Multipath error results summary for GPS L1 only

To be certain the previous results were not affected by the increased number of cycle slips at lower elevations (which reduces the number of available multipath measurements), results using a minimum of 50-second arcs (as opposed to 200 sec) were analyzed. Figure 14 summarizes these results showing increased multipath at low elevations. This means that the results in the previous L1-only results are affected by the lack of long arcs at low elevations. This also indicates an increase in cycle slips for low ENU (and body frame) elevation angles.

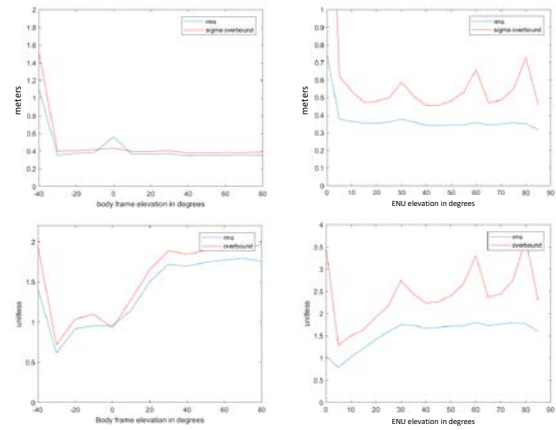


**Figure 14.** Multipath error results summary for GPS L1 only using 50-sec arcs.

### *Effect on Satellite Outages*

The attitude and orientation of the aircraft were used to analyze their correlation with satellite outages. Only outages that occurred in flight for satellites above 5° ENU elevation mask were considered. Further, to increase the available flight data for this analysis, it was assumed that a loss of L1 indicates a loss of the satellite.

GPS L1 data from 54 flights were examined to reveal a total of 165 outages. Of those, only 32 were above 5° ENU elevation angle. The median outage length was 6 seconds, and all but one of the outages occurred at a body frame elevation angle below 0°. Also, outages affected satellites that had as much as 15° (ENU) elevation. (See Figures 15 through 17.)

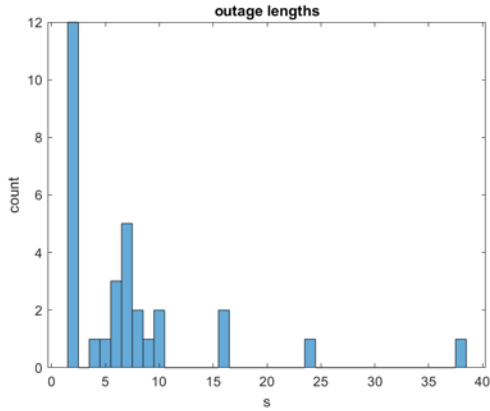


**Figure 15.** Number of outages as a function of outage length.

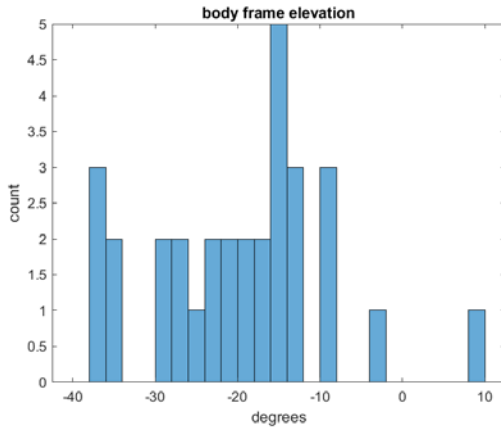


**Figure 16.** Number of outages as a function of body frame elevation angle.

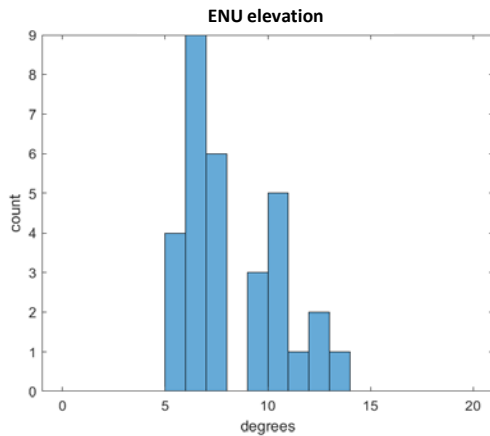
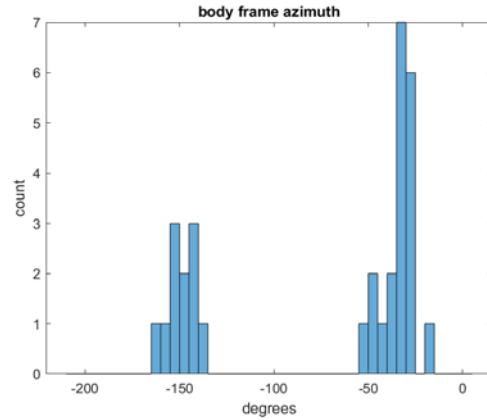


**Figure 17.** Outages as function of ENU elevation angle.

A coarse body frame azimuth was also computed. As mentioned previously, some errors in this estimate may arise from the assumption that the velocity is

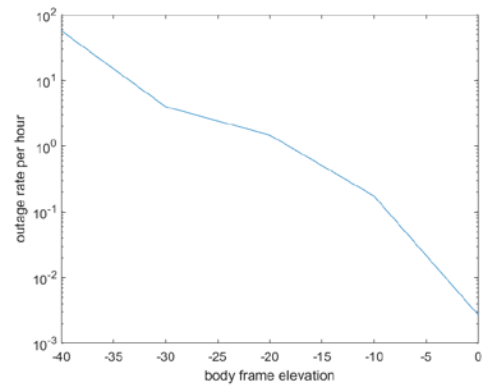
aligned with the aircraft body. (Crosswinds can cause the aircraft body to be offset with respect to the velocity, and this offset can be up to 30 degrees.)

Figure 18 plots the body frame azimuth outage results. It was observed that the outages occur at azimuths closer to  $0^\circ$  and  $-180^\circ$ —i.e., along the body of the aircraft. The observed asymmetry ( $-30^\circ$  and  $-150^\circ$ ) of this distribution could be due to a prevalence in the turn direction.



**Figure 18.** Outages as function of body frame azimuth angle.

When the outages are computed as a rate, a more informative trend can be seen. (See Figure 19.) The outage rate is very sensitive to banking angles. For negative body frame elevation angles the rate is quite high. Still, most satellites were tracked well below  $5^\circ$  body frame elevation. This may partially mitigate the effects of these banking induced outages (as compared to what availability simulation results may predict).



**Figure 19.** Outages as function of body frame azimuth angle.

### Effect on Cycle Slips

To evaluate the effect on cycle slip rate, the same approach as for the outage rate was taken. GPS L1, L5 and Galileo E1, E5a measurements from 17 flights were processed. All measurements were binned per body frame elevation angle. The rate was computed by counting the number of cycle slips and dividing it by the total number of measurements in that bin. (This translates the 1-Hz measurements directly to a rate of cycle slips per satellite-second).

The results for GPS L1-L5 and Galileo E1-E5a are plotted in Figures 20 and 21, respectively. As expected, the cycle slip rate follows a behavior similar to the outage rate. It greatly increases for negative body frame elevation angles. At the minimum elevation, the cycle slip rate reaches 1 per satellite-sec. If this rate were to occur on a single satellite signal, it is likely the code measurements could not be sufficiently smoothed, potentially inflating protection levels for extended periods of time.

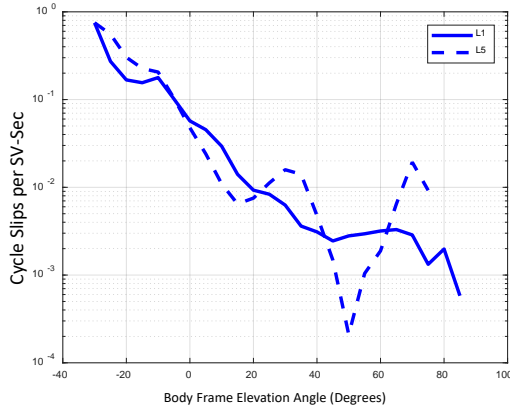


**Figure 20.** Cycle slip rate (per satellite-second) for GPS L1-L5

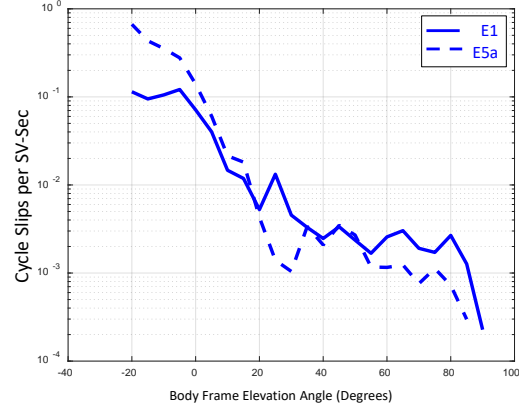


**Figure 21.** Cycle slip rate (per satellite-second) for Galileo E1-E5a

### Effect on ARAIM Performance

The Matlab Algorithm Availability Simulation Tool [5] was used to determine the effect of bank angle on ARAIM availability from outages. (Outages have the most significant impact, so effects from frequent cycle slips were not included in this analysis.) As a conservative step, it was assumed that the aircraft always has a 30-degree bank angle. Available satellites were then determined based on the apparent body frame elevation and azimuth, which both depend on the velocity direction. The worst case PLs were then taken for the velocity azimuths of 0 to 360 every 45 degrees. Any satellite with a negative body frame elevation and an azimuth between (-30° and 30°) and (150° and 210°) was assumed unavailable (based on the results from Figure 17).

Figures 22 and 23 plot the baseline (i.e., assuming straight and level flight) HPL and availability (respectively) for RNP 0.1 (HAL = 185m) with URA = 2.5 m. Figures 24 and 25 plot the corresponding worst case HPL and availability assuming 30° banking (with outages corresponding the prescribed azimuths). When large banking is assumed, the HPL increases from <40 m almost everywhere to up to 370 m in some regions, and the minimum availability decreases from 99.9% to 99%.

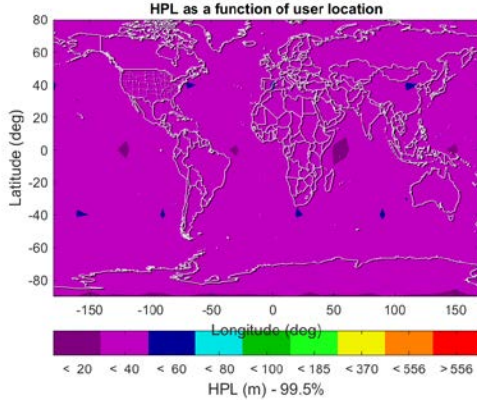


**Figure 22.** HPL (Baseline) as a function of user location for RNP 0.1. (GPS 24, Galileo 24 with URA=2.5 m,  $P_{\text{sat}} = 10^{-5}$ ,  $P_{\text{const,GPS}} = 10^{-8}$ , and  $P_{\text{const,Gal}} = 10^{-4}$ )

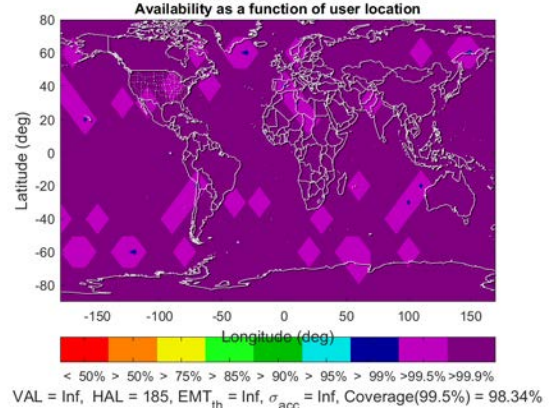


**Figure 25.** Availability (with 30° Bank Angle) as a function of user location for RNP 0.1. (GPS 24, Galileo 24 with URA=2.5 m,  $P_{\text{sat}}=10^{-5}$ ,  $P_{\text{const,GPS}}=10^{-8}$ , and  $P_{\text{const,Gal}} = 10^{-4}$ )

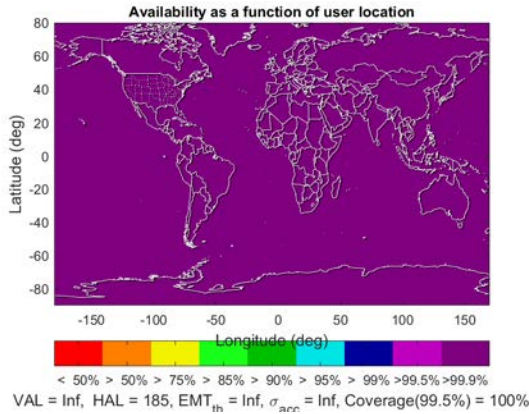


**Figure 23.** Availability (Baseline) as a function of user location for RNP 0.1. (GPS 24, Galileo 24 with URA=2.5 m,  $P_{\text{sat}} = 10^{-5}$ ,  $P_{\text{const,GPS}} = 10^{-8}$ , and  $P_{\text{const,Gal}} = 10^{-4}$ )

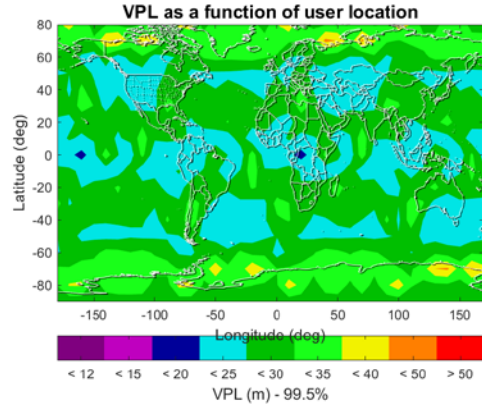


**Figure 26.** VPL (Baseline) as a function of user location for LPV-200. (GPS 24, Galileo 24 with URA=1.0 m,  $P_{\text{sat}} = 10^{-5}$ ,  $P_{\text{const,GPS}} = 10^{-8}$ , and  $P_{\text{const,Gal}} = 10^{-4}$ )

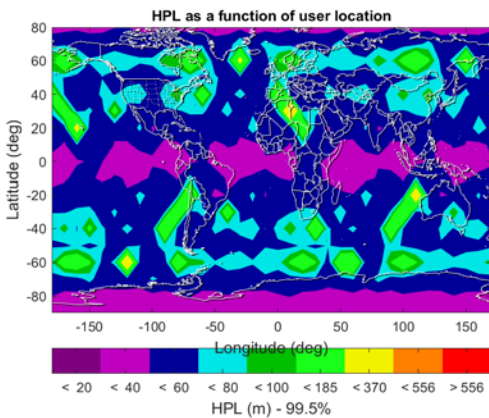


**Figure 24.** HPL (with 30° Bank Angle) as a function of user location for RNP 0.1. (GPS 24, Galileo 24 with URA=2.5 m,  $P_{\text{sat}} = 10^{-5}$ ,  $P_{\text{const,GPS}} = 10^{-8}$ , and  $P_{\text{const,Gal}} = 10^{-4}$ )

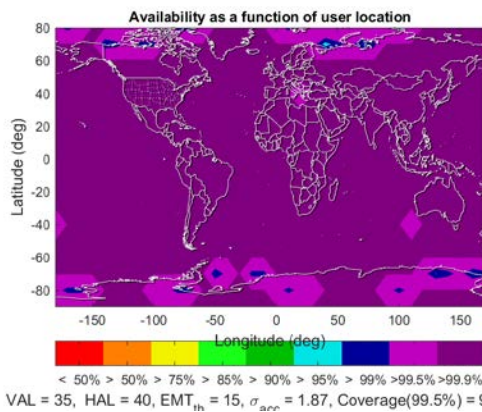


**Figure 27.** Availability (Baseline) as a function of user location for LPV-200. (GPS 24, Galileo 24 with URA=1.0 m,  $P_{\text{sat}} = 10^{-5}$ ,  $P_{\text{const,GPS}} = 10^{-8}$ , and  $P_{\text{const,Gal}} = 10^{-4}$ )

Figures 26 and 27 plot the baseline VPL and availability (respectively) for LPV-200 with URA = 1.0 m. Figures 28 and 29 plot the corresponding worst case VPL and availability assuming 30° banking. With banking, the VPL increases from between 25 and 30 meters most everywhere to a maximum that exceeds 50 meters in some regions. And the minimum availability decreases from >99.9% to as low as 95% in many places.

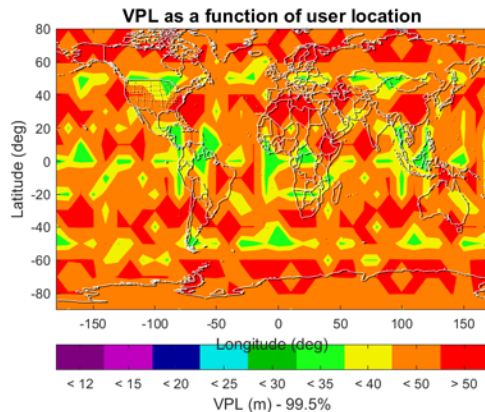


**Figure 28.** VPL (at 30° Bank Angle) as a function of user location for LPV-200. (GPS 24, Galileo 24 with URA=1.0 m,  $P_{\text{sat}} = 10^{-5}$ ,  $P_{\text{const,GPS}} = 10^{-8}$ , and  $P_{\text{const,Gal}} = 10^{-4}$ )

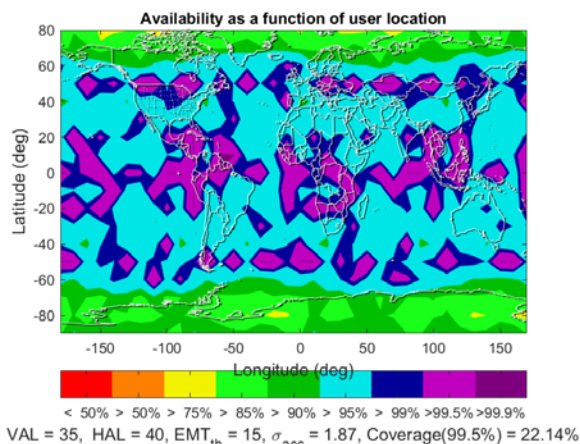


**Figure 29.** Availability (at 30° Bank Angle) as a function of user location for LPV-200. (GPS 24, Galileo 24 with URA=1.0 m,  $P_{\text{sat}}=10^{-5}$ ,  $P_{\text{const,GPS}}=10^{-8}$ , and  $P_{\text{const,Gal}} = 10^{-4}$ )

Note that while such severe banking (and corresponding outages) may not always be a condition that exists during approaches, it is possible for such maneuvers to take place for some aircraft just prior to an approach. And, since some outages may persist for

sometimes tens of seconds, they may have a measurable effect on availability well after the aircraft has leveled off.

## CONCLUSIONS

Flight data was used to characterize the effect of bank angle on GNSS signals. As expected, satellites that are masked by the aircraft may have more code multipath. However that increased multipath is largely accounted for by the elevation dependent multipath error model applied by ARAIM users. Aircraft banking may also cause a high maximum satellite outage rate. This contrasts with the standard assumptions that this rate is negligible during an approach. In addition, banking may significantly increase the rate of cycle slips. It was observed that rates increased to nearly one per second (over all satellites) for the largest banking angle (30°) observed.

Preliminary ARAIM availability simulations show that satellite outages due to large aircraft banking (at certain aircraft orientations) may have a significant impact on the baseline satellite configurations. And, if an outage persists beyond the duration of the maneuver, it may have a measurable effect on availability even after an aircraft has leveled off. While conditions are rare, and mitigations do exist for outages and other brief degradations in signal quality, it is believed such banking-induced effects should be considered when modeling performance for GNSS systems for aviation.

## REFERENCES

- [1] Working Group C, ARAIM Technical Subgroup, Milestone 3 Report, February 26, 2016. Available at: <http://www.gps.gov/policy/cooperation/europe/2016/working-group-c/>  
[http://ec.europa.eu/growth/tools-databases/newsroom/cf/itemdetail.cfm?item\\_id=8690](http://ec.europa.eu/growth/tools-databases/newsroom/cf/itemdetail.cfm?item_id=8690)
- [2] Phelts, R. Eric, Blanch, Juan, Chen, Yu-Hsuan, Enge, Per, Riley, Stuart, "ARAIM in Flight Using GPS and GLONASS: Initial Results from a Real-time Implementation," *Proceedings of the 29th International Technical Meeting of The Satellite Division of the Institute of Navigation (ION GNSS+ 2016)*, Portland, Oregon, September 2016, pp. 3264-3269.

[3] Blanch, Juan, Phelts, R. Eric, Chen, Yu-Hsuan, Enge, Per, "Initial Results of a Multi-Constellation ARAIM Airborne Prototype," *Proceedings of the 2017 International Technical Meeting of The Institute of Navigation*, Monterey, California, January 2017, pp. 184-209.

[4] WAAS Minimum Operational Performance Specification (MOPS), RTCA document DO-229D.

[5] Jan, SS., Chan, W. & Walter, T. GPS Solutions, September 2009, Vol. 13, No 4  
<https://doi.org/10.1007/s10291-009-0117-4>